

# RSC Advances



This is an *Accepted Manuscript*, which has been through the Royal Society of Chemistry peer review process and has been accepted for publication.

*Accepted Manuscripts* are published online shortly after acceptance, before technical editing, formatting and proof reading. Using this free service, authors can make their results available to the community, in citable form, before we publish the edited article. This *Accepted Manuscript* will be replaced by the edited, formatted and paginated article as soon as this is available.

You can find more information about *Accepted Manuscripts* in the [Information for Authors](#).

Please note that technical editing may introduce minor changes to the text and/or graphics, which may alter content. The journal's standard [Terms & Conditions](#) and the [Ethical guidelines](#) still apply. In no event shall the Royal Society of Chemistry be held responsible for any errors or omissions in this *Accepted Manuscript* or any consequences arising from the use of any information it contains.

# Textured Transparent Conductive B/Al doped ZnO Films Utilizing Reactive Magnetron Sputtering

Yang Liu, Qian Huang\*, Lisha Bai, Changchun Wei, Dekun Zhang and Xiaodan Zhang\*\*

*Institute of Photo Electronics Thin Film Devices and Technique of Nankai University, Key Laboratory of Photo Electronics Thin Film Devices and Technique of Tianjin, Key Laboratory of Optoelectronic Information Science and Technology, Ministry of Education, Tianjin 300071, China*

\*Corresponding author: [carolinehq@nankai.edu.cn](mailto:carolinehq@nankai.edu.cn)

\*\*Co-Corresponding author: [xdzhang@nankai.edu.cn](mailto:xdzhang@nankai.edu.cn)

## Abstract:

High-quality textured transparent conductive oxide (TCO) is significant to exceptional performance of solar cells. In this study, textured B/Al doped ZnO (ZnO:B/Al) films were firstly reported utilizing reactive RF magnetron sputtering from an intrinsic ZnO ceramic target in B<sub>2</sub>H<sub>6</sub>-Ar gas mixture. Elaborate thermal treatment was conducted for film optimization, as the temperature dependency of B<sub>2</sub>H<sub>6</sub> source was quite sensitive. A compound structure with 200-nm thick Al capping layer and 2000-nm thick ZnO:B main layer was proposed to further improve the annealing performance. The initial resistivity and mobility of reactive sputtered ZnO:B/Al film were  $4.8 \times 10^{-4} \Omega\text{cm}$  and  $32.1 \text{ cm}^2/\text{V}\cdot\text{s}$  respectively. A remarkable surface texture with root-mean-square higher than 170 nm was developed after a chemical etching procedure, resulting in average light scattering over 89% and total transmittance higher than 86% in the whole spectrum. These optical properties illustrate a prominent progress in TCO application in thin film silicon (TFS) solar cells. Preliminary microcrystalline silicon solar cells deposited on textured ZnO:B/Al films indicate  $0.6 \text{ mA}/\text{cm}^2$  enhancement in short-circuit current density compared to conventional ZnO:Al front contacts, indicating potential application in high-efficiency TFS solar cells.

**Keywords:** Transparent conductive oxides; Surface texture; Light Trapping; Thermal treatment; Thin-film solar cells

## 1. Introduction

Further development and implementation of efficient light management in high-performance thin film silicon (TFS) solar cells [1-6] are considered as the most important research area. In the *p-i-n* type solar cell deposited on TCOs, lights are introduced and trapped by the TCOs with high transmittance and textured-surface morphology. Thus, the performance of TCOs plays a crucial role in the high-efficiency TFS solar cells and forms a significant part of the photovoltaic research and development [5-7]. Two competing approaches to the fabrication of high-quality textured ZnO-based electrodes are: ZnO:Al mainly deposited by magnetron sputtering and ZnO:B mainly deposited by low pressure chemical vapor deposition (LPCVD). The former typically exhibits superior conductivity [2-4], while the latter possesses superior transparency at longer wavelengths [7-10].

ZnO:B films prepared by magnetron sputtering may provide an effective way to combine the advantages of conductivity and transparency [11-15]. Introducing B<sub>2</sub>H<sub>6</sub> into the sputtering atmosphere as a reactive doping source provides a feasible way to produce ZnO:B films [13-15]. The reactive sputtering may allow convenient regulation of doping concentration when sputtering is in progress. Hagiwara [13] et al. prepared ZnO:B films with resistivity of  $4.6 \times 10^{-4} \Omega\text{cm}$  by reactive RF magnetron sputtering from an undoped ZnO target in B<sub>2</sub>H<sub>6</sub>-Ar gas mixture. Superior optical properties relative to ZnO:Al films were exhibited. When applied as a window layer to CIGS solar cells, reactive sputtered ZnO:B was reported to yield higher quantum efficiencies compared to ZnO:Al films. Delahoy [15] et al. attained similar results with reactive hollow cathode sputtering from a metallic target in B<sub>2</sub>H<sub>6</sub>-O<sub>2</sub>-Ar gas mixture. Although the resistivity and transparency reported in the above work were competitive, effective scattering texture could not be obtained from the low deposition substrate temperature. This weakness results in challenges that reactive sputtered ZnO:B film encounter when it is applied in TFS solar cells.

Improvements in light scattering would allow the reactive sputtered ZnO:B films to possess effective conductivity, transparency, and light trapping simultaneously, thereby producing an effective candidate for high-performance of TFS solar cells. Surface texture realization of reactive sputtered ZnO:B films are reported for the first time in this study. Substrate temperature during deposition and thermal annealing procedure were precisely controlled to optimize the B<sub>2</sub>H<sub>6</sub> doping efficiency and crystalline quality. A compound structure with 200-nm thick Al capping layer and 2000-nm thick ZnO:B main layer (ZnO:B/Al) was then developed with significant

improvement in light scattering over the full spectrum. Potential application in high-efficiency thin-film solar cells was tested on this ZnO:B/Al front contact. To the best of our knowledge, this is the first time that reactive sputtered ZnO:B/Al films are used as the front contact in TFS solar cells.

## 2. Experiment

ZnO:B films were prepared on Corning eagle XG glass using RF magnetron sputtering from a ceramic intrinsic ZnO target in a KJLC Lab-18 sputtering system. B<sub>2</sub>H<sub>6</sub> was introduced into the chamber during the sputtering process as the doping source with a 5% dilution ratio (7 sccm Ar and 0.4 sccm B<sub>2</sub>H<sub>6</sub>). The sputtering chamber was maintained at a base pressure below  $2 \times 10^{-7}$  Torr prior to each deposition. The distance between the target and the substrate was maintained at 100 mm. Prior to each film deposition, the target was pre-sputtered in pure Ar (99.999%) at 5 mTorr to guarantee the repeatability. Low pressure (1.5 mTorr) and high power density (3.3 W/cm<sup>2</sup>) were utilized at different substrate temperatures. All ZnO:B samples were prepared with a thickness of approximately 2.0 μm.

A 200-nm-thick Al capping layer was then deposited onto the ZnO:B samples by *in situ* magnetron sputtering from a pure Al target to compose a ZnO:B/Al compound annealing film. *In situ* annealing process was then conducted for both ZnO:B and ZnO:B/Al films with various annealing temperatures for 2 hours in the Lab-18 sputtering system with a light source heater under a base pressure below  $2 \times 10^{-7}$  Torr. Prior to every measurement, the Al covering layer was removed by etching in NaOH solution. Finally, a post-deposition surface texturing was applied to provide effective coupling of light into TFS solar cells. By a wet chemical etching step in dilute hydrochloric acid (0.5% HCl), a texture of ZnO:B or ZnO:B/Al surface was obtained. The etching time was adapted to the specific properties of the deposited films.

In a preliminary study, sheet resistance was detected by a four-probe resistance test system. Film thicknesses were measured using a Dektak 3030 profilometer (Veeco Instruments Inc., Woodbury, USA). Resistivity, hall mobility, and carrier concentration were measured at room temperature using the van der Pauw method in the HL5500 Hall System (Accent, York, UK). Crystal quality was investigated by X-ray diffraction (D/max-2500/PC, Rigaku Inc., Japan). Film bonding states were analyzed by an Axis Ultra X-ray photoelectron spectrometer (Kratos Analytical Ltd, Manchester, UK) while the SUPRA 55VP scanning electronic microscopy (SEM)

(Carl ZEISS AG, Jena, Germany) and the SPA 400 atomic force microscopy (AFM) (SII Nanotechnology, Inc., Tokyo, Japan) were employed to characterize surface morphology. Perpendicular specular ( $T_{spe}$ ) and total transmittance ( $T_{tot}$ ) were measured using a Cary 5000 spectrophotometer (Varian Co., Palo Alto, USA) equipped with an integrated sphere in the 300-1200 nm spectrum range. Transmittance haze ( $H_T$ ) was determined as the fraction of diffuse (scattering angles exceeding  $5^\circ$ ) transmittance that constituted the total transmittance:  $H_T = [T_{tot} - T_{spe}] / T_{tot} \times 100\%$ .

### 3. Results and discussion

Original film microstructure affects surface texture after wet etching for sputtered ZnO films. Crystallization quality improvement consistently and positively contributes to obtaining a light trapping structure [16]. As the substrate temperature acts as a main influence factor in crystal quality, substrate temperature was adjusted from 50 to 200°C to optimize deposition procedure. Electrical properties of the as-grown ZnO:B samples are shown in Figure 1. For conventional sputtered ZnO:Al films, crystal quality improves along with higher temperature and tend to possess minimum resistivity above 300°C [2, 3]. However, a minimum resistivity of  $1.47 \times 10^{-3} \Omega\text{cm}$  is obtained for sputtered ZnO:B films with substrate temperature at 70°C. This low optimal substrate temperature indicates that  $B_2H_6$  is quite sensitive to thermal heating. Higher temperature diminishes the film carrier concentration and mobility obviously, as shown in Fig.1. We attribute this reduction to the re-evaporation of boron atoms and the formation of boron oxides or B-suboxide [17], as the substrate temperature further increases.

Thermal annealing provides a convenient method to improve crystal quality and conductivity [18-21]. In this study, ZnO:B films were deposited at 70°C followed by thermal annealing process at deferent temperature for 2 hours. The resistivity of annealed ZnO:B films appears to be optimized with annealing temperature at 320°C (ZnO:B-320), as shown in Fig. 2(a). Resistivity of  $5.1 \times 10^{-4} \Omega \cdot \text{cm}$  while carrier concentration of  $5.48 \times 10^{20} \text{cm}^{-3}$  and mobility of  $28.7 \text{ cm}^2/\text{Vs}$  are obtained. As annealing temperature is further increased, mobility is reduced along with the carrier concentration. Oxygen is a main driving force for the increase of resistivity, as described by different research groups focusing on doped ZnO annealing experiments [22, 23]. Experiments have demonstrated that a decrease in carrier concentrations

may be caused by the formation of oxygen interstitial [22]. Oxygen has also been suggested to decrease the mobility by chemisorption at grain boundaries, which enhances the contribution of grain boundary scattering [23].

Ruske *et al.* [21] described a silicon capping layer successfully prevented oxygen migration during the annealing step of ZnO:Al films. A 200-nm thick Al capping layer deposited by the *in situ* sputtering process was introduced prior to annealing in this study. With a 2-hour annealing treatment, samples with the Al cap exhibit higher tolerance on the annealing temperature without increase in resistivity. Detailed performance of the modified ZnO:B/Al annealing structure is shown in Fig. 2(b). As noted, the Al capping layer was removed prior to electrical measurements. At annealing temperature of 450°C, the ZnO:B/Al film (ZnO:B/Al-450) retains the lowest resistivity of  $4.8 \times 10^{-4} \Omega \cdot \text{cm}$  with carrier concentration of  $4.06 \times 10^{20} \text{ cm}^{-3}$  and mobility of  $32.1 \text{ cm}^2/\text{Vs}$ . As the substrate temperature exceeds 500°C, carrier concentration decreases, revealing that the formation of oxygen interstitial plays a major role for the annealed samples. Additionally, carrier concentration for annealed samples in the experiments is raised compared to the uncapped films, potentially as a result of extrinsic donor (Al) diffusion into the ZnO:B and passivation of acceptors states.

XPS data were then applied to verify the diffusion process. XPS survey spectra (0–1400 eV) on the initial surface of ZnO:B/Al-450 films were firstly produced before the high-resolution scan. Al, Zn, and O were identified in the spectra. Different thicknesses were etched away by dipping ZnO:B/Al-450 film into 0.5% HCl acid solution with different etching times. The calculated Al:Zn atomic percentage was extracted from the high resolution scan of Al 2p and Zn 2p<sub>3/2</sub> peaks in Tab. 1 for each thickness etched away. XPS data suggest that Al diffused into the ZnO:B film during the annealing process. With increasing depth, Al content decreased and then disappeared when etching thickness expanded beyond 1000 nm. The diffusion of Al must then affect the carrier concentration determined by Hall measurements, as Al atoms act as shallow donors in ZnO films.

XRD was conducted for samples under different annealing conditions. All samples exhibited a strong peak near 34.5° and a weak peak at 72.5°, associated with (002) and (004) planes of hexagonal phase, suggesting a polycrystalline structure with a preferred orientation of the c-axis perpendicular to the substrate. The variation of full-width at half-maximum (FWHM) values of (002) diffraction peak extracted from

XRD patterns and the grain size estimated according to the Scherrer formula are shown in Fig.3. The FWHM gradually decreases along with the increase of annealing temperature and reaches its minimum value of 0.32 degree for capped annealed ZnO:B/Al-450. Simultaneously, the grain size along the c-axis linearly increases from 22.71 nm for initial ZnO:B sample to 25.93 nm for ZnO:B/Al-450, which was annealed at 450°C. The improvement of crystallinity caused the highest mobility of 32.1 cm<sup>2</sup>/Vs of the annealed ZnO:B/Al-450 film, outstripping 19 cm<sup>2</sup>/Vs of the initial ZnO:B and 28.7 cm<sup>2</sup>/Vs of the annealed ZnO:B-320.

Optical property of the TCOs relates directly to the performance of the solar cell device. A high transparency in full spectrum normally results in high Jsc for TFS solar cell by reducing the parasitic light absorption. Fig. 4 illustrates the spectral transmittance in the wide spectrum range (300-1200 nm) for different samples. The presence of point defects, dislocations, impurities, grain boundaries, and its strain state play an important role in the absorption coefficient of a semiconductor thin film. Higher-temperature annealing process corresponded to transmittance promotion over the full spectrum and was related to the crystalline quality improvement with fewer defects. Red arrows in Fig. 4 show that the ZnO:B/Al-450 film resulted in high transmittance in both short and long wavelength range with a relatively high annealing temperature. The average transmittance extracted from 400 to 1100 nm was over 85% (containing a glass substrate with average transmittance of ~92%) and will be beneficial for  $\mu$ c-Si:H, a-SiGe:H and tandem/triple-junction solar cells.

A chemical-etching process was then conducted on the ZnO:B and ZnO:B/Al films annealed under different conditions to obtain the light-trapping morphology. Films were dipped into 0.5% HCl acid solution with different etching time to adapt specific properties of the deposited films. Within 10 seconds, the as-deposited ZnO:B film without annealing procedure was completely etched away. Because of this unconsolidated structure, the as-deposited ZnO:B film cannot perform obvious texture morphology during the wet etching process. After a 20-second or 32-second etching procedure, the clear transparent appearance of the ZnO:B-320 and ZnO:B/Al-450 films were changed to a milky one in diluted HCl acid, with sheet resistance of ~10 ohm/sq and thickness of ~800 nm. The etching rate decreases obviously along with increasing the annealing temperature. As the deviation of uniformity is less than 10% within the 5×5 cm<sup>2</sup> testing area, the etching rate does not show clear difference between the film center and edges.

Additionally, a conventional sputtered ZnO:Al film deposited at 325°C was dipped into the diluted HCl acid for 25 seconds as a reference. Changes in the surface morphology of ZnO:B-320, ZnO:B/Al-450, and AZO films were investigated by AFM as shown in Fig. 5. The initial smooth ZnO films before etching (ZnO:B-320 and ZnO:Al) do not show obvious difference in RMS roughness, which is less than 10 nm, as shown in Fig. 5 (a) and (c). The surface of initial ZnO:B/Al-450 film shows tiny texture with RMS roughness less than 30 nm, as shown in Fig. 5 (b), which could be related to the peeling step of Al covering layer by NaOH solution. Following the etching process, a typical crater-like surface structure can be clearly identified for each sample. Surface morphology with RMS roughness of 148 nm of the etched conventional AZO film, as shown in Fig. 5 (f), are on the concurrently comparable level to AZO films reported by other groups [2,16].

The etched ZnO:B-320 film appears in a moderately textured topography with lateral sizes of 1-2  $\mu\text{m}$  and RMS roughness of 124 nm (Fig. 5 (d)). The ZnO:B/Al-450 film shows enlarged surface features with RMS roughness of 172 nm, which is related to crystal quality improvement as supported by the XRD features. Unclear boundaries could then be potentially identified with more elaborate surface structure [Fig. 5 (e)]. The details of surface morphology characterized by SEM (Fig. 6) identifies a complicated structure for etched ZnO:B/Al-450 film. A moderately textured topography has been developed with a wide range of crater-like surface features and large craters (3~4  $\mu\text{m}$ ) uniformly distributed on the surface embedded by small ones (< 1  $\mu\text{m}$ ).

Special surface morphology of etched ZnO:B/Al-450 film is attributed to thermal diffusion of Al atoms during annealing process. The density and compactness of ZnO films are affected by Al atom profiling in the top and bottom layer[24] and results in different etching properties depending on the Al arrangement. The top layer tends to form larger size pits while the bottom layer tends to form smaller pits during the etching process. This special surface morphology is shown in Fig. 7 and indicates that large craters formed at first, followed by small crater formation in the large craters during the etching process.

Total transmittance ( $T_{\text{tot}}$ ), and haze factor ( $H_T$ ) of the texture-etched films are illustrated in Fig. 8. High transmittance is exhibited by all of the films in the visible and infrared region. Textured ZnO:B/Al-450 sample shows exceptional transmittance over the whole spectrum with high average total transmittance over 86% extracted

from 400 to 1100 nm. The average  $H_T$  value from 400 to 1100 nm is 89.5% with  $H_T$  of 88% at the wavelength of 850 nm, demonstrating a remarkable 20% and 25% improvement compared to the annealed ZnO:B-320 and ZnO:Al films, respectively. Effective scattering is associated with a wide range of crater-like surface features and the special morphology of small craters inside big craters allows improved light scattering in the whole solar spectrum [25].

Finally, we emphasize the potential application of the textured ZnO:B film as a transparent electrode in TFS solar cell. Co-deposited single  $\mu\text{-Si:H}$  cells are prepared on conventionally etched AZO and ZnO:B/Al-450 front contacts. The i-layer thickness of these  $\mu\text{-Si:H}$  cells was 1.5  $\mu\text{m}$  with a high deposition rate of 15  $\text{\AA/s}$ . To study the electrical performance and wavelength dependence of the cell characteristics, current density voltage (JV) and external quantum efficiency (EQE) measurements were performed.

Taking ZnO:B/Al-450 as the front contact in  $\mu\text{-Si:H}$  solar cells, the higher EQE in the entire wavelength region resulted in a 0.6  $\text{mA/cm}^2$  enhancement of the short-circuit current density, as shown in Fig. 9 (a). Enhanced light transmittance and scattering increased the optical flux and path length, and is beneficial to the current density. Unfortunately, a few narrow and sharp valleys can be identified by AFM or SEM images (Fig.5 and Fig. 6) in the ZnO:B/Al films, which tends to cause nanoporous defective phase (commonly termed as “cracks” or “voids”) in the initial deposition of  $\mu\text{-Si:H}$  layers. These defects inevitably lead to the current leakage of solar cells and then both the  $V_{oc}$  and FF decrease [26,27], as shown in Fig.9 (b). To avoid this disadvantage, one effective way is to treat the ZnO:B/Al substrate by plasma to create smoother U-type surface [28]. Another potential method is to use p-type and n-type nc-SiOx:H doped layers [29,30]. All of these improvement will be tested in our future study to obtain high efficiency based on this ZnO:B/Al structure.

#### 4. Conclusion

Textured ZnO:B/Al films deposited from reactive magnetron sputtering are extensively studied. Thermal annealing conditions including substrate temperature and extra Al capping layer were selected to modify the structural and light trapping performance. Experimental results indicate that the ZnO:B/Al combined with a 200-nm thick Al capping layer is effective to protect against oxygen diffusion during annealing procedure. The treated film exhibits resistivity of  $4.8 \times 10^{-4} \Omega\text{cm}$  with total

transmittance substantially exceeding 86%. Remarkable RMS roughness higher than 170 nm and scattering haze of over 89% in full spectrum could be obtained by the etching procedure presented here. Textured reactive sputtered ZnO:B/Al films may function as optimum front contacts for solar cells with excellent conductivity, transparency and light trapping properties simultaneously in full spectrum.

### **Acknowledgements**

This work was supported by the National Basic Research Program of China (2011CBA00706), National Natural Science Foundation of China (61404074, 61474065), Research Program of Application Foundation and Advanced Technology of Tianjin (14JCQNJC02100), Tianjin Research Key Program of Application Foundation and Advanced Technology (15JCZDJC31300), Key Project in the Science & Technology Pillar Program of Jiangsu Province (BE2014147-3) and Specialized Research Fund for the PhD Program of Higher Education (20120031110039).

## References

- [1] Y. H. Kim, J. S. Kim, W. M. Kim, T. Y. Seong, J. Lee, L. Müller-Meskamp, K. Leo, Realizing the Potential of ZnO with Alternative Non-Metallic Co-Dopants as Electrode Materials for Small Molecule Optoelectronic Devices, *Adv. Funct. Mater.* 23 (2013) 3645–3652.
- [2] M. Berginski, J. Hüpkes, M. Schulte, G. Schöpe, H. Stiebig, B. Rech, The effect of front ZnO:Al surface texture and optical transparency on efficient light trapping in silicon thin-film solar cells, *J. Appl. Phys.* 101 (2007) 074903-1–074903-11.
- [3] J. Müller, B. Rech, J. Springer, M. Vanecek, TCO and light trapping in silicon thin film solar cells, *Sol. Energy* 77 (2004) 917–930.
- [4] S. Kim, J. W. Chung, H. Lee, J. Park, Y. Heo, H. M. Lee, Remarkable progress in thin-film silicon solar cells using high-efficiency triple-junction technology, *Sol. Energy Mater. Sol. Cells* 119 (2013) 26–35.
- [5] O. Isabella, J. Krc, and M. Zeman, Modulated surface textures for enhanced light trapping in thin-film silicon solar cells, *Appl. Phys. Lett.* 97 (2010) 101106-1–101106-3.
- [6] V. E. Ferry, M. A. Verschuuren, M. C. V. Lare, R. E. I. Schropp, H. A. Atwater, and A. Polman, Optimized Spatial Correlations for Broadband Light Trapping Nanopatterns in High Efficiency Ultrathin Film a-Si:H Solar Cells, *Nano Lett.* 11 (2011) 4239-4245.
- [7] J. Escarré, K. Söderström, M. Despeisse, S. Nicolay, C. Battaglia, G. Bugnon, L. Ding, F. Meillaud, F.-J. Haug, and C. Ballif, Geometric light trapping for high efficiency thin film silicon solar cells, *Solar Energy Materials & Solar Cells.* 98 (2012) 185-190
- [8] A. Hongsingthong, I. A. Yunaz, S. Miyajima, and M. Konagai, Preparation of ZnO thin films using MOCVD technique with D<sub>2</sub>O/H<sub>2</sub>O gas mixture for use as TCO in silicon-based thin film solar cells, *Sol. Energy Mater. Sol. Cells* 95 (2011) 171-174.
- [9] L. Ding, M. Boccard, G. Bugnon, M. Benkhaira, S. Nicolay, M. Despeisse, F. Meillaud, and C. Ballif, Highly transparent ZnO bilayers by LP-MOCVD as front electrodes for thin-film micromorph silicon solar cells, *Solar Energy Materials & Solar Cells.* 98 (2012) 331-336
- [10] S. Fay, J. Steinhauser, S. Nicolay, C. Ballif, Polycrystalline ZnO: B grown by LPCVD as TCO for thin film silicon solar cells, *Thin Solid Films* 518 (2010) 2961-2966
- [11] L. Gao, Y. Zhang, J. M. Zhang, K. W. Xu, Boron doped ZnO thin films fabricated by RF-magnetron sputtering, *Applied Surface Science* 257 (2011) 2498-2502.

- [12] Q. Huang, Y. Wang, S. Wang, D. Zhang, Y. Zhao, X. Zhang, Transparent conductive ZnO: B films deposited by magnetron sputtering, *Thin Solid Films* 520 (2012) 5960-5964.
- [13] Y. Hagiwara, T. Nakada, A. Kunioka. Improved Jsc in CIGS thin film solar cells using a transparent conducting ZnO:B window layer. *Solar Energy Materials & Solar Cells* 67 (2001) 267-271
- [14] T. Nakada, Y. Ohkubo, N. Murakami, et al. Transparent Conducting Boron-Doped Zinc Oxide Films Deposited by DC-Magnetron Sputtering in B<sub>2</sub>H<sub>6</sub>-Ar Mixtures. *Japanese Journal of Applied Physics* 34 (1995) 3623-3627
- [15] A.E. Delahoy, S. Y. Guo, Transparent and semitransparent conducting film deposition by reactive environment, hollow cathode sputtering. *Journal of Vacuum Science & Technology A* 23 (2005) 1215-1220
- [16] O. Kluth, G. Schöpe, J. Hüpkes, C. Agashe, J. Müller, and B. Rech, Modified Thornton model for magnetron sputtered zinc oxide: film structure and etching behavior, *Thin Solid Films*. 442 (2003) 80-85
- [17] L.H. Long, The mechanisms of thermal decomposition of diborane and of interconversion of the boranes: A reinterpretation of the evidence, *Journal of Inorganic and Nuclear Chemistry* 32 (1970) 1097-1115
- [18] Z. B. Fang, Z.J. Yan, Y.S. Tan, X.Q. Liu, Y.Y. Wang, Influence of post-annealing treatment on the structure properties of ZnO films, *Appl. Surf. Sci.* 241 (2005) 303-308
- [19] T. Minami, T. Hirano, T. Miyata, and J. Nomoto, Influence of rapid thermal annealing on surface texture-etched Al-doped ZnO films prepared by various magnetron sputtering methods, *Thin Solid Films* 520 (2012) 3803-3807
- [20] N. Ohta, D. Ohba, S. Sato, Z. Tang, H. Shimizu, H. Shirai, Rapid thermal-plasma annealing of ZnO:Al films for silicon thin-film solar cells, *Thin Solid Films* 519 (2011) 6920-6927
- [21] F. Ruske, M. Roczen, K. Lee, M. Wimmer, S. Gall, J. Hüpkes, D. Hrunski, and B. Rech, Improved electrical transport in Al-doped zinc oxide by thermal treatment, *Journal of Applied Physics* 107 (2010) 013708-1–013708-8.
- [22] J. H. Noh, H. S. Jung, J.-K. Lee, J. Y. Kim, C. M. Cho, J. An, and K. S. Hong, Reversible change in electrical and optical properties in epitaxially grown Al-doped ZnO thin films, *J. Appl. Phys.* 104 (2008) 0737068-1–0737068-5.

- [23] T. Minami, T. Miyata, and T. Yamamoto, Stability of transparent conducting oxide films for use at high temperatures, *J. Vac. Sci. Technol. A* 17 (1999) 1822-1826.
- [24] C. Agashe, O. Kluth, J. Hüpkes, U. Zastrow, B. Rech and M. Wuttig, Efforts to improve carrier mobility in radio frequency sputtered aluminum doped zinc oxide films, *Journal of Applied Physics* 95 (2004) 1911-1917
- [25] Y. Wang, X. Zhang, L. Bai, Q. Huang, C. Wei, .Y. Zhao, Effective light trapping in thin film silicon solar cells from textured Al doped ZnO substrates with broad surface feature distributions, *Appl. Phys. Lett.* 100 (2012) 263508-1–263508-4.
- [26] H.B.T. Li, R.H. Franken, J.K. Rath, R.E.I. Schropp, Structural defects caused by a rough substrate and their influence on the performance of hydrogenated nano-crystalline silicon n-i-p solar cells, *Sol. Energy Mater. Sol. Cells*, 93 (3) (2009) 338–349.
- [27] Y. Nasuno, M. Kondo, A. Matsuda, Effects of substrate surface morphology on microcrystalline silicon solar cells, *Jpn. J. Appl. Phys. Lett.*, 40 (2001) L303–L305
- [28] M. Addonizio, A. Antonaia, Surface morphology and light scattering properties of plasma etched ZnO: B films grown by LP-MOCVD for silicon thin film solar cells, *Thin Solid Films*, 518 (4) (2009) 1026–1031.
- [29] M. Despeisse, C. Battaglia, M. Boccard, G. Bugnon, M. Charrière, P. Cuony, S. Hänni, L. Löfgren, F. Meillaud, G. Parascandolo, T. Söderström, C. Ballif, Optimization of thin film silicon solar cells on highly textured substrates, *Phys. Status Solidi A* 208(8) (2011) 1863–1868.
- [30] M. Despeisse, G. Bugnon, A. Feltrin, M. Stuckelberger, P. Cuony, M. Meillaud, A. Billet, C. Ballif, Resistive interlayer for improved performance of thin film silicon solar cells on highly textured substrate. *Applied Physics Letters* 96(7) (2010) 073507.

**Tables:**

Table 1. The calculated Al:Zn atomic percent extracted from the high resolution scan of Al 2p and Zn 2p<sub>3/2</sub> peaks for ZnO:B/Al-450 films with different thickness removed. (The thickness of as-deposited ZnO:B/Al-450 film was 1820 nm)

Thickness removed from ZnO:B/Al-450 (nm)	0	435	648	1004
Al: Zn (at%)	15.13	10.63	7.64	0

Figures:

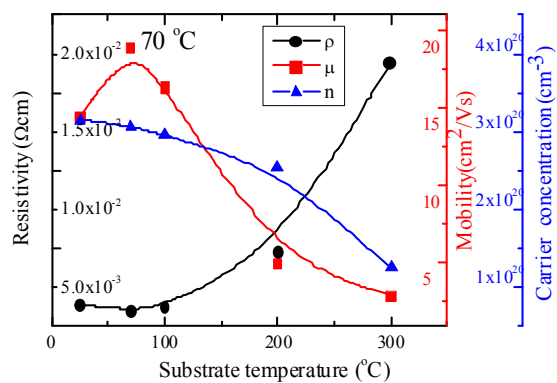
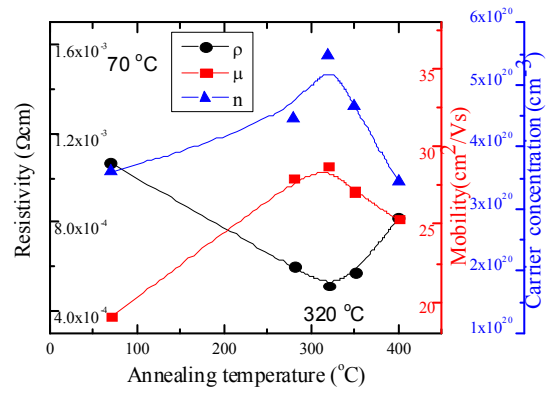
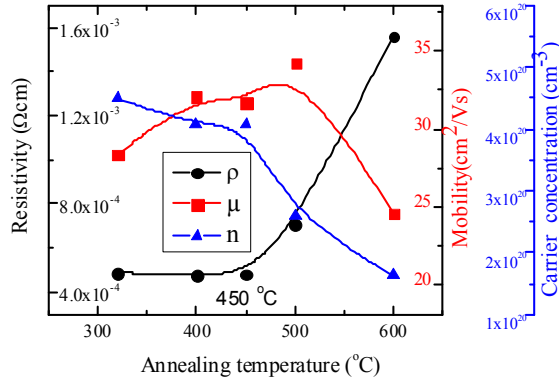


Fig. 1 Electrical properties of ZnO:B films deposited at different substrate temperatures

(Resistivity: black circle; Mobility: red square; Carrier concentration: blue triangle)



(a)



(b)

Fig. 2 Resistivity of ZnO:B films annealed at different temperatures (a) without Al capping layer

(b) with Al capping layer

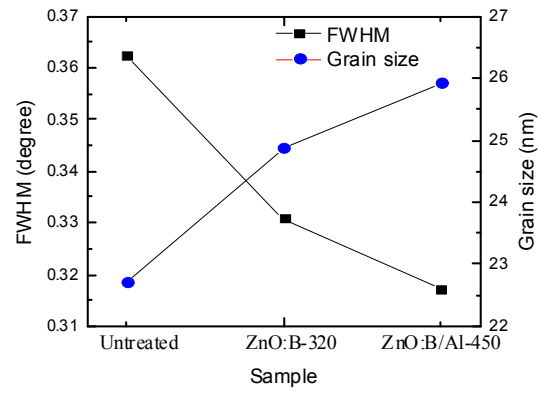


Fig. 3 FWHM of (002) diffraction peak and grain size of samples under different annealing condition

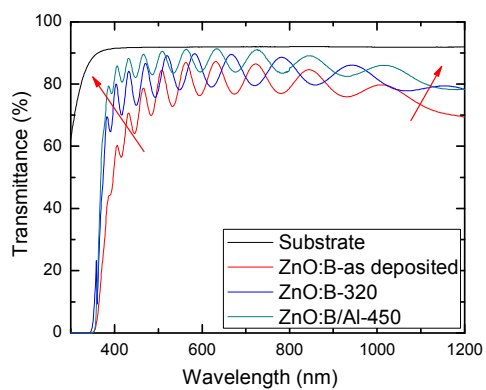


Fig. 4 Spectral transmittance of ZnO:B films annealed at different temperatures (Red arrows show that the ZnO:B/Al-450 film resulted in high transmittance both in short and long wavelength range)

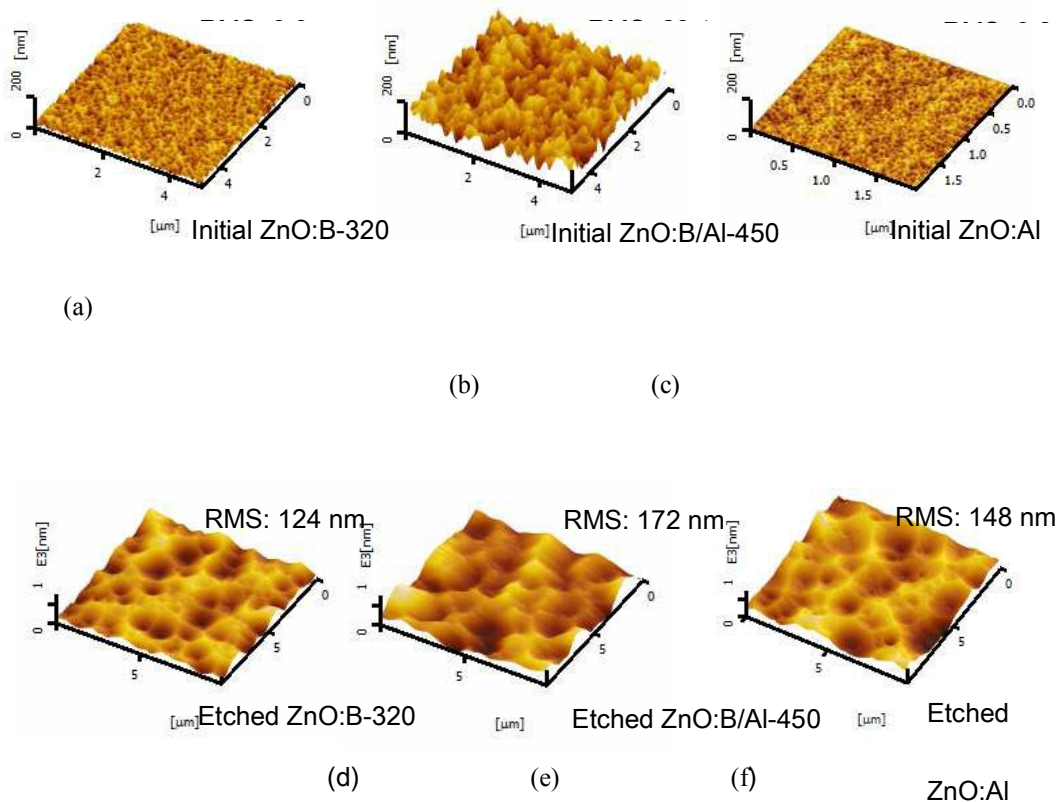


Fig. 5 Three-dimensional atomic force microscopy images of the initial and etched films (a) initial ZnO:B film annealed at 320 °C (b) initial ZnO:B/Al film annealed at 450 °C (c) initial conventional ZnO:Al film deposited at 325 °C as a reference (d) etched ZnO:B film annealed at 320 °C (e) etched ZnO:B/Al film annealed at 450 °C (f) etched conventional ZnO:Al film deposited at 325 °C

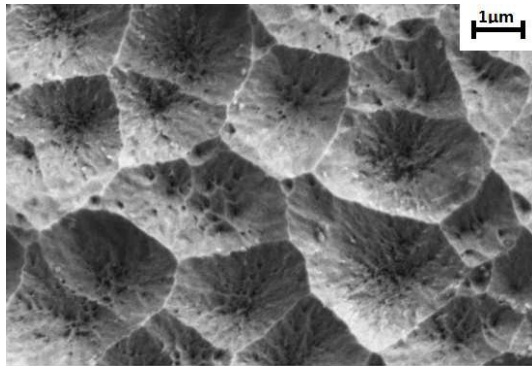


Fig. 6 SEM image of capped annealing ZnO:B/Al-450 film

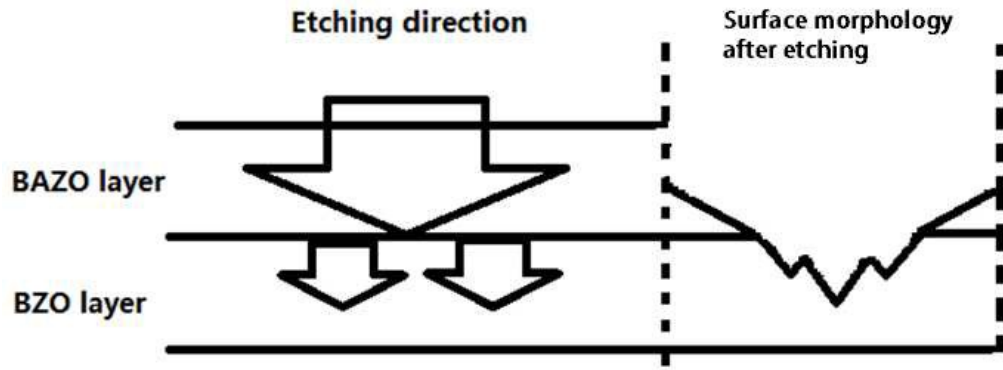


Fig. 7 Schematic illustration of the etching process of capped annealing ZnO:B films

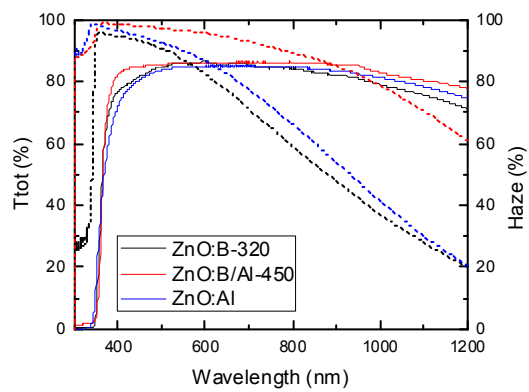
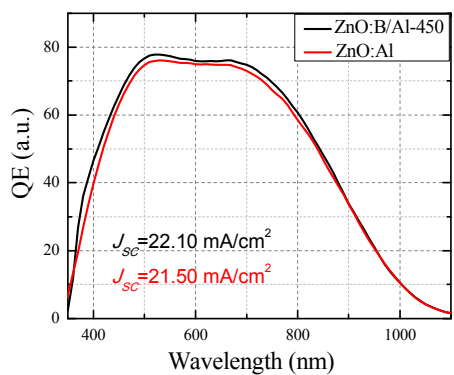
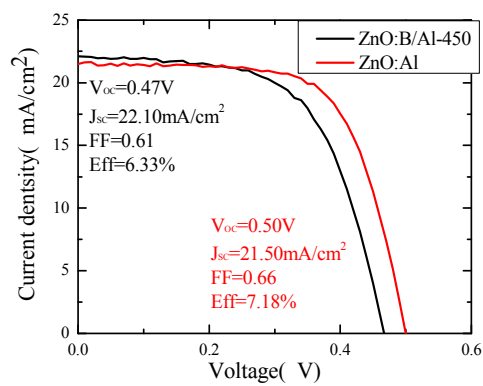


Fig. 8 Total transmittance ( $T_{tot}$ , solid line) and Haze factor ( $H_T$ , dashed line) of the etched

ZnO:B-320, ZnO:B/Al-450 and ZnO:Al films



(a)



(b)

Fig. 9 EQE and J-V curves of the  $\mu\text{c-Si:H}$  solar cells that were deposited on the standard

ZnO:Al and ZnO:B/Al-450 front contacts

(a) EQE curves of  $\mu\text{c-Si:H}$  solar cells; (b) J-V curves of  $\mu\text{c-Si:H}$  solar cells